Published in final edited form as:

Curr Biol. 2017 October 09; 27(19): 3010–3016.e3. doi:10.1016/j.cub.2017.08.036.

Retrotransposons mimic germ plasm determinants to promote transgenerational inheritance

Bhavana Tiwari[1], **Paula Kurtz**[1], **Amanda Jones**[1], **Annika Wylie**[1], **James Amatruda**[2,3,4], **Devi Prasad Boggupalli**[5], **Graydon B. Gonsalvez**[5], and **John M. Abrams**[*,1]

[1]Department of Cell Biology, University of Texas Southwestern Medical Center, Dallas, Texas 75390, USA

[2]Department of Pediatrics, University of Texas Southwestern Medical Center, Dallas, Texas 75390, USA

[3]Department of Molecular Biology, University of Texas Southwestern Medical Center, Dallas, Texas 75390, USA

[4]Department of Internal Medicine, University of Texas Southwestern Medical Center, Dallas, Texas 75390, USA

[5]Cellular Biology and Anatomy, Medical College of Georgia, Augusta University, 1459 Laney Walker Blvd, Augusta, GA 30912, USA

SUMMARY

Retrotransposons are a pervasive class of mobile elements present in the genomes of virtually all forms of life [1, 2]. In metazoans these are preferentially active in the germline, which, in turn, mounts defenses that restrain their activity [3, 4]. Here we report that certain classes of retrotransposons insure transgenerational inheritance by invading presumptive germ cells before they are formed. Using sensitized *Drosophila* and zebrafish models, we found that diverse classes of retrotransposons migrate to the germ plasm, a specialized region of the oocyte that prefigures germ cells and specifies the germline of descendants in the fertilized egg. In *Drosophila*, we found evidence for a 'stowaway' model, whereby *Tahre* retroelements traffic to the germ plasm by mimicking *oskar* RNAs and engaging the Staufen-dependent active transport machinery. Consistent with this germ plasm determinants attracted retroelement RNAs, even when these components were ectopically positioned in bipolar oocytes. Likewise, vertebrate retrotransposons

[*]Correspondence: john.abrams@utsouthwestern.edu.
[*]Lead Contact

Author Contributions

B.T. designed experiments, carried out experiments, analyzed data and composed the manuscript. J.M.A. designed experiments, analyzed the data and contributed to manuscript composition. G.G. helped design experiments, analyze the data and gave critical suggestions. D.P.B performed *in situ* hybridization and image acquisition on *oskar* RNA and protein null strains, Tm1C and Khc deplete strains. P.K. helped conceive the study, interpret the data and conducted initial experiments. A.J. and A.W. contributed pivotal unpublished data particularly for the zebrafish studies. J.F.A. helped design experiments, interpret the data and made critical technical contributions for the zebrafish studies.

similarly migrated to the germ plasm in zebrafish oocytes. Together, these results suggest that germ plasm targeting represents a fitness strategy adopted by some retrotransposons to insure transgenerational propagation.

Graphical Abstract

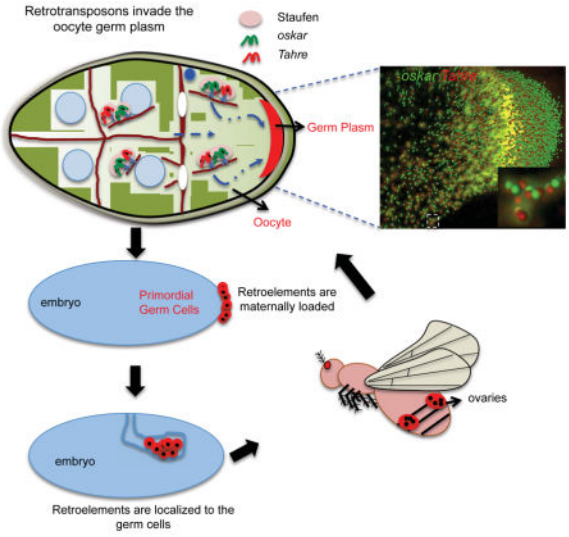

RESULTS AND DISCUSSION

Tahre retroelements migrate to the oocyte germ plasm

In the *Drosophila* ovary, retrotransoposon RNAs are often transcribed in neighboring nuclei and subsequently migrate to the oocyte. For example, Factor *I* retrotransposon RNAs produced in nurse cells migrate to the oocyte nucleus [5–7] and, likewise, *Gypsy I* RNAs produced in follicle cells traverse the perivitelline membrane to access the oocyte [6, 8, 9].

Recently, we discovered that p53 restrains mobile elements, raising the possibility that $p53^{-/-}$ genotypes could expose properties of transposons that are otherwise below detection limits [10–12]. Using this sensitized genetic background, we observed localization of *Tahre* retroelements to a posterior cortical region of the fly oocyte, consistent with possible migration to the so-called germ plasm [10]. To confirm this interpretation, we compared *Tahre* RNA localization patterns with well studied *oskar* and *nanos* RNAs. As a pioneer factor that initiates germ plasm formation, *oskar* transcripts migrate to the posterior region of the oocyte in mid oogenesis using an active and uniquely dedicated pathway [13]. Subsequently, *nanos* transcripts are recruited to this structure during the later stages of oogenesis [13, 14]. *In situ* hybridization experiments revealed early and efficient posterior localization of *Tahre* transcripts that mirrored *oskar* RNAs in oocytes of stage 9–10 egg chambers from $p53^{-/-}$ females. As shown in Figures 1A, *Tahre* localization patterns were virtually identical to *oskar* patterns and preceded the gradient of *nanos* transcripts seen in later-staged oocytes (Figure S1C). These studies demonstrated accumulation of *Tahre* retroelement in the $p53^{-/-}$ germ plasm (Figure 1A) (see also Figures S1B and 1C) and affirmed that little or no *Tahre* was detected in WT oocytes (see Figure S1A).

oskar RNAs migrate from nurse cells to the oocyte posterior in ribonucleoparticles (RNPs) [15]. To determine if *Tahre* RNAs were co-packaged in these granules, we quantified pairwise co-localization of *Tahre* with either *oskar* or *nanos* RNAs (See STAR Methods). Co-localization of *Tahre* and *oskar* (0.43) was significantly higher than *Tahre* and the *gapdh* control (.004) (Figure 1B) or *Tahre* and *nanos* (see Figure S1C) indicating *Tahre* transcripts often (but not always) co-localized with *oskar* RNAs. Furthermore, our co-localization analyses of *oskar* and *Tahre* RNAs in early (Figure S1G) and later-staged egg chambers (Figure S1H) suggested that co-packaging of *Tahre* RNAs in *oskar* RNPs initiates when these particles exit the nurse cell nuclei. As these cargoes traversed the oocyte, coincident signals steadily increased and peaked at the posterior cortical region (Figure S1I). Hence, as *Tahre* transcripts migrate to the posterior pole they were often - but not always - transported with the pioneer factor that initiates germ plasm assembly [16, 17].

To ask whether the germ plasm is itself sufficient to attract *Tahre* transcripts, we examined *Tahre* localization in samples expressing engineered *oskar* RNAs, (*oskar-bcd*3′UTR) that are misdirected to the anterior pole of developing oocytes by virtue of a bicoid (*bcd*) localization signal [18]. In these egg chambers, ectopic localization and translation of *oskar-bcd*3′UTR transcripts at the anterior pole triggers germ plasm formation, resulting in so-called ‘bipolar oocytes’ containing germ plasms at both the anterior (ectopic) and posterior (normal) pole [19]. As seen in Figures 1C, *Tahre* retroelements localized to both poles of these oocytes, exhibiting characteristic bipolar patterns that continued through the later stages of oogenesis and persisted in early embryos as well (Figure S1E, F). Together, these studies established that the germ plasm, rather than the posterior cortex, is sufficient to attract retrotransposons.

The *oskar* transport machinery conveys *Tahre* to the germ plasm

Staufen is an RNA binding protein required for transport of *oskar* RNAs to the posterior pole of the oocyte [20, 21]. *Tahre* contains very long 3′UTRs, which is an important feature of Staufen bound transcripts [22]. Therefore, we hypothesized that Staufen might also be required to transport *Tahre* RNAs to the germ plasm. To test this possibility, we inspected localization of *Tahre* and *oskar* patterns in Staufen$^{-/-}$p53$^{-/-}$ [*staufen*^{HL}/*staufen*^{ry9}; p53$^{-/-}$] ovaries. Upon loss of Staufen [20, 21], *oskar* RNAs failed to localize to the germ plasm region as expected (Figures 2A and 2B). Likewise, when *staufen* was defective, *Tahre* retroelements similarly failed to localize (Figures 2C, 2D, S2A and S2B) and equivalent results were observed in RNAi strains depleted for *staufen* (see Figures S2 E–H). Importantly, like *oskar* RNAs (see Figure S2C), mislocalized *Tahre* transcripts (Figure 2D) accumulated at the anterior boundary of *staufen*-depleted oocytes. Furthermore, these retroelement RNAs were often - but not always - colocalized with *oskar* containing RNPs that were similarly mislocalized (Figure S2D).

Staufen contains five RNA binding domain (RBD) motifs [23]. One domain, RBD2 is known to be crucial for the posterior localization of *oskar* transcripts but another domain, RBD5 is dispensable [21]. To investigate whether RBD2 is similarly required for localization of retroelement RNAs, we visualized *Tahre* transcripts using *staufen* alleles mutated for either the RBD2 or RBD5 and quantified *Tahre* RNAs using our FISH assays. As seen in Figures S2, the RBD2 of Staufen was critical for migration of *Tahre* to the germ

plasm region while the RBD5 was dispensable (Figures S2I–K). Therefore, not only is Staufen required to transport *Tahre* to the germ plasm, but *Tahre* localization also requires the same RNA binding domain needed to convey *oskar* transcripts. Using the same approach, we also examined other factors that transport *oskar* RNAs, including kinesin (Figures S3D and S3E), and its interacting partner Tropomyosin1C (Tm1C) (Figures S3F and S3G), [24–26]. Here we observed that *Tahre* and *oskar* were similarly mislocalized, providing further support for the idea that these RNAs target the germ plasm region using shared molecular machinery.

Trafficking of *oskar* RNAs that form the germ plasm is mediated by physical association with Staufen protein. Therefore, to test whether *Tahre* retroelements might similarly complex with Staufen we used complementary methods. First, using a tagged allele of Staufen [27] we found extensive co-localization with *Tahre* RNAs, at the germ plasm (Figures 2F). Second, we performed RNA immunoprecipitation (RIP) assays and detected significant binding of *Tahre* retroelements to Staufen. As seen in Figures 2G and 2H, these interactions were comparable to binding of Staufen to *oskar* RNAs [22], which served as our benchmark for these studies. Furthermore, these interactions were specific, since neither *nanos* (posteriorly localizing) nor *act42A* mRNAs were enriched (Figures 2G and 2H). Together, these observations suggest that *Tahre*, like *oskar*, physically associates with Staufen to reach the presumptive germ plasm.

Tahre retroelements persist in germ cells of the next generation

Tahre retroelements are co-transported with *oskar* RNPs in a Staufen-dependent manner, suggesting that these selfish elements may target the germ plasm as a fitness strategy that insures transmission to the F2 generation. To evaluate this possibility, we determined whether *Tahre* RNAs persisted in the germline of the F1 generation by inspecting recently fertilized embryos prior to the onset of zygotic expression. We observed *Tahre* transcripts localized to the pole plasm of precellularized embryos (see Figure S4E–G) as well as at the pole cells of the cellularized embryos (Figures 3A and S4A). We used *nanos* transcripts to mark embryonic pole cells (Figure S4B) in these studies and, as seen in Figure S4C, *Tahre* and *nanos* RNAs were extensively co-localized. Hence, these retroelement RNAs are transmitted from the oocyte germ plasm to the embryo and, furthermore, these maternally derived transcripts persist in the presumptive germ cells of the F1 blastula. To genetically verify this maternal effect, we inspected early embryos produced from either $p53^{+}$ or $p53^{-}$ mothers. In these reciprocal out crosses, maternally loaded *Tahre* RNAs appeared only in samples produced from $p53^{-}$ mothers, as expected (Figure S4D). Hence, *Tahre* retroelements can invade the germline of subsequent generations by targeting of the oocyte germ plasm. Furthermore, as shown in Figures 3B and 3C, we also detected *Tahre* transcripts in the primordial gonads of later staged embryos (stage 8), suggesting that these maternally loaded mobile elements persist in the differentiated germline of descendants.

Migration of retrotransposons to the germ plasm is a conserved phenomenon

To ask whether germ plasm targeting by retroelements is a broadly conserved phenomenon we surveyed other classes of *Drosophila* retroelements. Like *Tahre* retroelements, *Burdock* and *HeT-A* also localized to the oocyte germ plasm (Figures 4A–F and see also Table S1)

and, similarly, *Burdock* RNAs (see Figures S4H–I) persisted in the pole plasm of precellularized embryos. In contrast, other retroelements such as *Idefix* were not localized to germ plasm. Hence, some but not all classes of *Drosophila* retrotransposons target the germ plasm and persist in pole cells.

To determine whether germ plasm targeting might also occur in vertebrate systems, we examined developing oocytes in zebrafish and, as above, we used $p53^{-/-}$ mutants as a sensitized background. In preliminary studies, we profiled native retroelements that erupt in early $p53^{-/-}$ zebrafish embryos (A.W. and A.J., unpublished observations) and, among these, we selected *Gypsy54* for FISH analyses, since this retroelement was highly derepressed in $p53^{-/-}$ ovaries (Figure 4G). Using *Gypsy54*-specific probes, we observed that these RNAs localized to the Balbiani body, an aggregate of mitochondria, Golgi and endoplasmic reticulum [28, 29] that marks the germ plasm of zebrafish oocytes at this stage (Figure 4H). The Balbiani body is present in oocytes of all animals including mammals [30, 31] and can be routinely detected by staining with DiOC6 [32]. Therefore, to confirm our interpretation, we conducted FISH experiments followed by DiOC6 staining and, as seen in Figures 4H–J, *Gypsy54* transcripts accumulated in the germ plasm of these early oocytes (Figure 4J), co-localizing with DiOC6-stained Balbiani bodies at high penetrance (Figure 4K). In later staged oocytes, the germ plasm migrates to the cortical region [33] and, as seen in Figure 4I, *Gypsy54* transcripts similarly localized to these positions as well. Hence, retroelements present in vertebrate genomes can target the oocyte germ plasm. We also followed *Gypsy54* RNAs after fertilization prior to zygotic transcription and, in these studies, we detected localization to the cleavage planes of 4 cell stage embryos (Figure S4N). Since gametes form at these positions [34], our results suggest that, as in flies, retroelement RNAs can persist in the presumptive gametes of the F1 generation.

Conclusion

We found that diverse classes of retrotransposons migrate to - and accumulate in - the germ plasm, a structure within the oocyte that prefigures germ cells and ultimately specifies the germline of F1 descendants. In this way, certain mobile elements appear to invade rudimentary components of germ cells that eventually form ‘grandchildren’ through the maternal lineage. Hence, germ plasm targeting could represent a fitness strategy that promotes transmission in subsequent generations and, at the same time, may evade un-necessary costs associated with transposition in somatic cells [35]. We found compelling support for this in our case study of the *Drosophila Tahre* retroelement. First, RNA coded by this transposon mirrored the migratory behaviors of both native and ectopic *oskar* RNAs, which specify germ plasm formation. Second, germ plasm targeting by *Tahre* required at least three factors (Staufen, kinesin heavy chain and Tm1C) that normally enable *oskar* RNAs to construct the germ plasm. Third, *Tahre* RNAs physically associated with Staufen, recruiting the same machinery (Figures S2 and S3) and RNA binding domain (Figure S2I and S2J) needed to transport *oskar* RNAs.

An attractive explanation for these observations proposes that *Tahre* transcripts mimic *oskar* RNAs, acting as molecular stowaways to gain passage from their site of production in nurse cells to the oocyte germ plasm. Consistent with this, we found that *Tahre* RNAs were indeed

co-packaged within *oskar* granules (Figures S1G–I) that are transported by the Staufen complex. Since *oskar* RNAs multimerize within RNPs [36], it is plausible that *Tahre* retroelements indirectly associate with Stafuen by tethering to *oskar* RNAs en route to the posterior pole. However, we favor direct physical binding to Staufen for two reasons. First, in both normal and perturbed settings we infrequently, but consistently, observed RNPs that contained *Tahre* RNAs but lacked detectable *oskar* RNAs (e.g. Figure S1H). Second, *Tahre* retroelements were decoupled from germ plasm accumulation of *oskar* RNAs in stage 10 osk^{84} oocytes that lacked Oskar protein (see Figure S3C, where *oskar* RNAs accumulated in the germ plasm region but *Tahre* retroelements did not). While *Tahre* mislocalization in these mutants could reflect a role for Oskar protein, more likely explanations for this phenotype trace to the absence of a germ plasm in osk^{84} oocytes [37, 38]. Nevertheless, taken together, these observations suggest that co-packaging with *oskar* transcripts is often incidental but is not required to transport *Tahre* to the germ plasm.

Together, our observations provide compelling evidence that *Tahre* retrotransposons use molecular mimicry to traffic to the germ plasm by co-opting a pathway dedicated to forming this structure. Consistent with this, germ plasm targeting is a property shared by other retroelements in *Drosophila* and in zebrafish (Figures 4 and S4E–M). Furthermore, transposon RNAs in the oocyte germ plasm persisted in the germline progenitors of the next generation (Figures S4E–N) and, in the case of *Tahre*, these likely perdured in gametes of these descendants. Since other retrotransposons migrate to the oocyte nucleus [5–7], this work illustrates how diverse retrotransposons can adopt different propagation strategies by targeting distinct subcellular components within the oocyte.

Retrotransposons and their host genomes exert reciprocal selective pressures that are often exposed in reproductive contexts, including oogenesis. Since *Tahre* elements support telomere formation [39], the need to maintain telomeres could potentially drive germ plasm targeting. However, this explanation is not generally satisfying since other retrotransposons with no role in telomere function also migrate to the germ plasm (e.g., *Burdock* in flies, *Gypsy54* in zebrafish). In closing, it is tempting to speculate that some mobile elements may have contributed to the evolution of germline specification by targeting the germ plasm in some lineages. Consistent with this, evolutionary models teach that transposons “tend to create, and then to sharpen, distinctions between the germline and soma” [40]. Considering the evidence presented here we believe this is a plausible scenario.

STAR METHODS

CONTACT FOR REAGENT AND RESOURCE SHARING

Further information and requests for protocols and datasets should be directed to and will be fulfilled by the Lead Contact, John Abrams (john. abrams@utsouthwestern.edu).

EXPERIMENTAL MODEL AND SUBJECT DETAILS

Fly stocks were maintained at 22°C–25°C on standard food medium. Two $p53^{-/-}$ null alleles, $p53^{-/-}$, 238H (ns) and 5A-1-4 (k1), were used in transcombination. For comparison, yw and w1118 were used in transcombination. For knockdown studies, *staufen UAS-RNAi*

(BL#43187) were obtained from the Bloomington Stock Center (Indiana University, Bloomington, IN) and crossed with 238H (ns). The driver line *gal4-nanos* (BL#4442) was crossed with 5A-1-4 (k1) to generate p53 mutations. *staufen*^{HL} (BL#1507) and *staufen*^{ry9} (BL#10742) [20], were crossed with 5A-1-4 (k1) to generate p53 mutations, and used in (transcombinations). Mutant stocks *stau*^{D3}*, P{w+, staufenΔRBD5}/CyO; stau*^{D3}*, P{w+, staufenΔloop2}, sp/CyO* [21] were crossed with *staufen*^{HL} (BL#1507) to visualize *Tahre* localization. w;pUASp-*oskar* (CDNA, w^{+})-*bcd*3′UTR;PrDr/Tm3,Ser [19] was a kind gift from Dr. Ruth Lehmann, The Howard Hughes Medical Institute, The Skirlball Institute of Biomolecular Medicine, Newyork University School of Medicine, were crossed with p53 null strains to generate p53 mutation.

METHOD DETAILS

***In situ* hybridization on *Drosophila* ovaries—**Stellaris probes (Biosearch Technologies) were designed, to detect the *Tahre*, *Gypsy*, *Burdock*, *HeT-A*, *oskar* and *nanos* mRNAs, using the Biosearch design tool (Table S2). Quasar 570-conjugated Stellaris oligonucleotide probes against *gapdh* were obtained from LGC Biosearch Technologies (Petaluma, CA). Ovaries were hybridized with the Stellaris RNA FISH probe sets following the manufacturer's instructions. Briefly, ovaries were dissected into PBS and fixed for 35 min at room temperature with 4% formaldehyde solution in PBS. After fixation, ovaries were placed in 70% ethyl alcohol overnight at 4°C. The following day, the ethyl alcohol was aspirated, and wash buffer (2x SSC, 10% deionized formamide in nuclease-free water) was added for 5 min. The probe was diluted at a concentration of 50 nM in hybridization buffer (2x SSC, 10% dextran sulfate [Sigma, D8906], 1 mg/mL tRNA [Sigma, R8759], 2 mM vanadyl robonucleoside complex [New England Biolabs], 10% deionized formamide (in nuclease free water). Hybridization solution with probes was added to each sample which were then placed at 37°C for 24 h. The samples were then washed with wash buffer twice for 15 min each at 37°C. Vecta Shield (Vector Laboratories) with DAPI was added before mounting and imaging. For Figure S3, RNA *in situ* hybridization was followed as described in [25].

Immunostaining of fly ovary—Well-fed females were dissected in PBS and fixed in 4% formaldehyde (Thermo scientific, 28908) diluted in PBS–0.1% Triton X-100 (PBST) and three volumes of heptane. After washing, tissues were blocked in 1.5% BSA and then incubated with 1:250 GFP antibody (rabbit, Invitrogen Molecular Probes, A11122) overnight at 4°C and probed with Alexa-488 (Invitrogen) secondary antibody. After washing, ovaries were mounted in Vecta Shield (Vector Laboratories) for imaging.

***Drosophila* embryo collections and *in situ* hybridization—**Embryos (0–2 h) were collected from WT (yw/w^{1118}) and p53$^{-/-}$ (k1/ns) strains on standard grapes juice agar plates with yeast paste. RNA *in situ* hybridizations were performed using manufacturers (Stellaris) protocol. Embryos were dechorionated in ~50% bleach for 2 minutes and washed thoroughly with double distilled H_2O. Embryos were transferred to a scintillation vial-containing fixative (1ml 4% PBS and 4ml heptane) and vortexed for 25 min. The embryos at the bottom were collected and rinsed with methanol 3 times and stored in methanol

overnight prior to *in situ* hybridization. The same protocol was used on 0–3 h and 2–6 h embryos to analyze pole cells and primordial gonad cells respectively.

***In situ* hybridization on Zebrafish embryos and ovaries—**Zebrafish of the AB and *tp53*$^{M214K/M214K}$ [41] strains were used for these experiments. Stellaris probes (Biosearch Technologies) were designed to detect the *Gypsy54* mRNAs using the Biosearch design tool. Sequence of zebrafish *Gypsy54* was obtained from Repbase [42]. Probes were labeled with Quasar 570; sequences are listed in Table S2. 2–4 cell-staged embryos were washed in 1X PBS and fixed in 4% EM-grade paraformaldehyde (Electron Microscopy Sciences) overnight at 4°C. Fixed embryos were wash ed in 1X PBS and hand-dechorionated. After washing in 1X PBS, embryos were stored in 100% methanol at least one day, and rehydration of embryos were carried out as described in [43]. Hybridization protocols, hybridization buffer and washing buffer were used as described for *Drosophila* ovary and embryos.

For *in situ* hybridization on ovary, WT and p53$^{-/-}$ fish were euthanized with an overdose of Tricaine. A small portion of the ovary was removed and stored in TRIzol for RNA isolation. The remainder of the ovary was fixed *in situ* in the fish overnight in 4% PFA/1X PBS at 4°C. Fixed ovaries were dissected out and and stored in 100% methanol at –20°C for at least 24 hours. On the third day, ovaries were rehydrated as described before for the Zebrafish embryos. Ovaries were digested with prewarmed proteinase K solution at 37°C for 30 min and digestion was stopped by incubating in 4% PFA in 1X PBST 5 min, followed by 4 washes with PBST. Ovaries were prehybridized in hybridization buffer for 2–5 hours at 37°C. Next, Hybridization buffer was removed and hybridization buffer containing probes and then incubated at 37°C for 24 h. The samples were then washed with wash buffer twice for 15 min each at 37°C. DiOC6 staining was performed with 5ng/ml DiOC6 (Invitrogen, D273) in 1X PBS for 10 minutes in rotating condition at room temperature. The ovaries were washed with 1X PBS 3 times; Vecta Shield (Vector Laboratories) without DAPI was added before mounting and imaging.

RNA Immunoprecipitation assay—A modified version of the protocol described in [44] was used with some modifications. Dissected ovaries were cross-linked using 0.08% formaldehyde in 1X PBS for 10 min and fixation was quenched with glycine. The ovaries were then placed on ice and rinsed with 1X PBS and followed by radioimmunoprecipitation assay (RIPA) buffer (50 mM Tris-HCl, 200 mM NaCl, 0.4% NP-40, 0.5% sodium deoxycholate, 0.1% SDS, 2 mM EDTA, 200 mM NaCl). The samples were lysed in RIPA plus (RIPA, 2.5 mg/ml yeast tRNA, 1 mM PMSF, 50 U/ml Roche RNAse inhibitor) and clarified by centrifugation. Supernatant was collected and mixed with either mixed with either anti-Staufen or anti-goat IgG antibodies and incubated at 4°C for 12 h followed by addition of protein A/G agarose beads (Santa Cruz). Samples were then incubated for 4 h at 4°C under constant rotation. The beads were then washed with 500 μl of RIPA plus U (RIPA plus supplemented with 1 M urea) and incubated in 1 mM Tris-HCl (pH 6.8), 5 mM EDTA, 10 mM DTT, 1.0% SDS at 70 °C for 45 min. Proteinase K was added to a final concentration of 0.1 mg/ml and samples were incubated for 25 min at 37°C. RNA was isolated using TRIzol, cDNA synthesis was performed using an iScript kit. Quantification

was performed with digital droplet PCR (BIORAD) using Eva Green supermix on a QX200 droplet reader. All concentration values for RIP assay targets were normalized either to IgG or unfixed samples. Primers used in this study were adapted from [10, 45]

Microscopy—Images were captured using 20X and 40X oil objectives with a Zeiss LSM 780 and LSM 880 inverted confocal microscopes and were prepared for presentation using the Fiji software package.

QUANTIFICATION AND STATISTICAL ANALYSIS

Co-localization analyses—For each experiment, image stacks were acquired from 3–5 different egg chambers/oocytes at each developmental stage shown. Images were taken at 0.3 μm intervals throughout the egg chamber using Zeiss LSM 880 inverted confocal microscope. For comparative analyses, acquisition settings were identical for all datasets. Images were deconvolved using the blind deconvolution algorithm of Autoquant X (Media Cybernetics). Co-localization was evaluated quantitatively using the coloc module of Imaris (Bitplane). Intensity thresholds of 500 was set and applied to all datasets. Co-localization statistics for each two-channel pair were obtained as csv files and analyzed with prism7 software. For upper limits of co-localization Quasar 570 and 670-labelled probes targeting overlapping regions on *Tahre* mRNAs were generated and cohybridized. For negative control, *Tahre* probes labeled-670 was co-hybridized with *gapdh* probe labeled with *Quasar 570*. As controls for the upper limits of co-localization, we co-hybridized *Tahre* probes, labeled with Quasar 570 and 670 (see Figure S1B). In addition, as a negative control, we also hybridized *Tahre* probes with a probe for *gapdh* (a non posterior localizing mRNA) (see Figure S1D). Pairwise co-localization of the two transcripts was measured by calculating the Pearson's coefficient in colocalized volume [46] using Imaris 8.0 (Biplane) software from and plotted using Prism7 software.

Supplementary Material

Refer to Web version on PubMed Central for supplementary material.

Acknowledgments

B.T. was supported by the CPRIT training grant to UT Southwestern. This work was supported by grants to PK (1F31GM108472-04), AW (NRSA 1F31CA189691-01), AEJ (ACS 128847-PF-15-160-01-DDC), GBG (R01GM100088), JFA (NIH R01CA135731 and CPRIT RP110394) and JMA (NIH R01GM072124, R01GM115682, and the Welch Foundation I-1865). GFP-Staufen, *staufenΔRBD2* and *staufenΔRBD5* strains were a kind gift from Andrea H. Brand Ph.D., from Wellcome/CRC Institute and Department of Genetics; Cambridge. Stocks obtained from the Bloomington *Drosophila* Stock Center (NIH P40OD018537) were used in this study. We thank the University of Texas Southwestern Live Cell Imaging Core, especially Kate Luby-Phelps Ph.D. and Abhijit Bugde, for assisting in microscopy and co-localization analyses. We would like to acknowledge Angelica Sanchez Ph.D. (J. Amatruda Lab at UTSW) for help in Zebrafish RNA *in situ* hybridization experiments. We thank Varsha Bhargava (M. Buszczak lab at UTSW) for advice on the RIP assay. We also thank Dr. Nicholas Conrad Department of Microbiology at UTSW for his helpful discussions.

References

1. Hua-Van A, Le Rouzic A, Maisonhaute C, Capy P. Abundance, distribution and dynamics of retrotransposable elements and transposons: similarities and differences. Cytogenet Genome Res. 2005; 110:426–440. [PubMed: 16093695]

2. Biemont C, Vieira C. Genetics: junk DNA as an evolutionary force. Nature. 2006; 443:521–524. [PubMed: 17024082]
3. van den Hurk JA, Meij IC, Seleme MC, Kano H, Nikopoulos K, Hoefsloot LH, Sistermans EA, de Wijs IJ, Mukhopadhyay A, Plomp AS, et al. L1 retrotransposition can occur early in human embryonic development. Hum Mol Genet. 2007; 16:1587–1592. [PubMed: 17483097]
4. Zamudio N, Bourc'his D. Transposable elements in the mammalian germline: a comfortable niche or a deadly trap? Heredity (Edinb). 2010; 105:92–104. [PubMed: 20442734]
5. Seleme MC, Disson O, Robin S, Brun C, Teninges D, Bucheton A. In vivo RNA localization of I factor, a non-LTR retrotransposon, requires a cis-acting signal in ORF2 and ORF1 protein. Nucleic Acids Res. 2005; 33:776–785. [PubMed: 15687386]
6. Van De Bor V, Hartswood E, Jones C, Finnegan D, Davis I. gurken and the I factor retrotransposon RNAs share common localization signals and machinery. Dev Cell. 2005; 9:51–62. [PubMed: 15992540]
7. Hamilton RS, Hartswood E, Vendra G, Jones C, Van De Bor V, Finnegan D, Davis I. A bioinformatics search pipeline, RNA2DSearch, identifies RNA localization elements in *Drosophila* retrotransposons. RNA. 2009; 15:200–207. [PubMed: 19144907]
8. Song SU, Kurkulos M, Boeke JD, Corces VG. Infection of the germ line by retroviral particles produced in the follicle cells: a possible mechanism for the mobilization of the gypsy retroelement of *Drosophila*. Development. 1997; 124:2789–2798. [PubMed: 9226450]
9. Touret F, Guiguen F, Terzian C. Wolbachia influences the maternal transmission of the gypsy endogenous retrovirus in *Drosophila* melanogaster. MBio. 2014; 5:e01529–01514. [PubMed: 25182324]
10. Wylie A, Jones AE, D'Brot A, Lu WJ, Kurtz P, Moran JV, Rakheja D, Chen KS, Hammer RE, Comerford SA, et al. p53 genes function to restrain mobile elements. Genes Dev. 2016; 30:64–77. [PubMed: 26701264]
11. Wylie A, Jones AE, Abrams JM. p53 in the game of transposons. Bioessays. 2016; 38:1111–1116. [PubMed: 27644006]
12. Levine AJ, Ting DT, Greenbaum BD. P53 and the defenses against genome instability caused by transposons and repetitive elements. Bioessays. 2016; 38:508–513. [PubMed: 27172878]
13. Becalska AN, Gavis ER. Lighting up mRNA localization in *Drosophila* oogenesis. Development. 2009; 136:2493–2503. [PubMed: 19592573]
14. Forrest KM, Gavis ER. Live imaging of endogenous RNA reveals a diffusion and entrapment mechanism for nanos mRNA localization in *Drosophila*. Curr Biol. 2003; 13:1159–1168. [PubMed: 12867026]
15. Mhlanga MM, Bratu DP, Genovesio A, Rybarska A, Chenouard N, Nehrbass U, Olivo-Marin JC. In vivo colocalisation of oskar mRNA and trans-acting proteins revealed by quantitative imaging of the *Drosophila* oocyte. PLoS One. 2009; 4:e6241. [PubMed: 19597554]
16. Lehmann R. Germ Plasm Biogenesis--An Oskar-Centric Perspective. Curr Top Dev Biol. 2016; 116:679–707. [PubMed: 26970648]
17. Mahowald AP. Assembly of the *Drosophila* germ plasm. Int Rev Cytol. 2001; 203:187–213. [PubMed: 11131516]
18. Macdonald PM, Struhl G. cis-acting sequences responsible for anterior localization of bicoid mRNA in *Drosophila* embryos. Nature. 1988; 336:595–598. [PubMed: 3143913]
19. Ephrussi A, Lehmann R. Induction of germ cell formation by oskar. Nature. 1992; 358:387–392. [PubMed: 1641021]
20. St Johnston D, Beuchle D, Nusslein-Volhard C. Staufen, a gene required to localize maternal RNAs in the *Drosophila* egg. Cell. 1991; 66:51–63. [PubMed: 1712672]
21. Micklem DR, Adams J, Grunert S, St Johnston D. Distinct roles of two conserved Staufen domains in *oskar* mRNA localization and translation. EMBO J. 2000; 19:1366–1377. [PubMed: 10716936]
22. Laver JD, Li X, Ancevicius K, Westwood JT, Smibert CA, Morris QD, Lipshitz HD. Genome-wide analysis of Staufen-associated mRNAs identifies secondary structures that confer target specificity. Nucleic Acids Res. 2013; 41:9438–9460. [PubMed: 23945942]
23. St Johnston D, Brown NH, Gall JG, Jantsch M. A conserved double-stranded RNA-binding domain. Proc Natl Acad Sci U S A. 1992; 89:10979–10983. [PubMed: 1438302]

24. Gaspar I, Sysoev V, Komissarov A, Ephrussi A. An RNA-binding atypical tropomyosin recruits kinesin-1 dynamically to oskar mRNPs. EMBO J. 2017; 36:319–333. [PubMed: 28028052]
25. Veeranan-Karmegam R, Boggupalli DP, Liu G, Gonsalvez GB. A new isoform of *Drosophila* non-muscle Tropomyosin 1 interacts with Kinesin-1 and functions in oskar mRNA localization. J Cell Sci. 2016; 129:4252–4264. [PubMed: 27802167]
26. Brendza RP, Serbus LR, Duffy JB, Saxton WM. A function for kinesin I in the posterior transport of oskar mRNA and Staufen protein. Science. 2000; 289:2120–2122. [PubMed: 11000113]
27. Palacios IM, St Johnston D. Kinesin light chain-independent function of the Kinesin heavy chain in cytoplasmic streaming and posterior localisation in the *Drosophila* oocyte. Development. 2002; 129:5473–5485. [PubMed: 12403717]
28. Billett FS, Adam E. The structure of the mitochondrial cloud of Xenopus laevis oocytes. J Embryol Exp Morphol. 1976; 36:697–710. [PubMed: 188969]
29. Heasman J, Quarmby J, Wylie CC. The mitochondrial cloud of Xenopus oocytes: the source of germinal granule material. Dev Biol. 1984; 105:458–469. [PubMed: 6541166]
30. Cox RT, Spradling AC. Milton controls the early acquisition of mitochondria by *Drosophila* oocytes. Development. 2006; 133:3371–3377. [PubMed: 16887820]
31. Pepling ME, Wilhelm JE, O'Hara AL, Gephardt GW, Spradling AC. Mouse oocytes within germ cell cysts and primordial follicles contain a Balbiani body. Proc Natl Acad Sci U S A. 2007; 104:187–192. [PubMed: 17189423]
32. Marlow FL, Mullins MC. Bucky ball functions in Balbiani body assembly and animal-vegetal polarity in the oocyte and follicle cell layer in zebrafish. Dev Biol. 2008; 321:40–50. [PubMed: 18582455]
33. Kosaka K, Kawakami K, Sakamoto H, Inoue K. Spatiotemporal localization of germ plasm RNAs during zebrafish oogenesis. Mech Dev. 2007; 124:279–289. [PubMed: 17293094]
34. Yoon C, Kawakami K, Hopkins N. Zebrafish vasa homologue RNA is localized to the cleavage planes of 2- and 4-cell-stage embryos and is expressed in the primordial germ cells. Development. 1997; 124:3157–3165. [PubMed: 9272956]
35. Haig D. Transposable elements: Self-seekers of the germline, team-players of the soma. Bioessays. 2016; 38:1158–1166. [PubMed: 27604404]
36. Little SC, Sinsimer KS, Lee JJ, Wieschaus EF, Gavis ER. Independent and coordinate trafficking of single *Drosophila* germ plasm mRNAs. Nat Cell Biol. 2015; 17:558–568. [PubMed: 25848747]
37. Kim-Ha J, Smith JL, Macdonald PM. oskar mRNA is localized to the posterior pole of the *Drosophila* oocyte. Cell. 1991; 66:23–35. [PubMed: 2070416]
38. Jenny A, Hachet O, Zavorszky P, Cyrklaff A, Weston MD, Johnston DS, Erdelyi M, Ephrussi A. A translation-independent role of oskar RNA in early *Drosophila* oogenesis. Development. 2006; 133:2827–2833. [PubMed: 16835436]
39. Shpiz S, Kwon D, Uneva A, Kim M, Klenov M, Rozovsky Y, Georgiev P, Savitsky M, Kalmykova A. Characterization of *Drosophila* telomeric retroelement TAHRE: transcription, transpositions, and RNAi-based regulation of expression. Mol Biol Evol. 2007; 24:2535–2545. [PubMed: 17890237]
40. Johnson LJ. Selfish genetic elements favor the evolution of a distinction between soma and germline. Evolution. 2008; 62:2122–2124. [PubMed: 18507740]
41. Berghmans S, Murphey RD, Wienholds E, Neuberg D, Kutok JL, Fletcher CD, Morris JP, Liu TX, Schulte-Merker S, Kanki JP, et al. tp53 mutant zebrafish develop malignant peripheral nerve sheath tumors. Proc Natl Acad Sci U S A. 2005; 102:407–412. [PubMed: 15630097]
42. Bao W, Kojima KK, Kohany O. Repbase Update, a database of repetitive elements in eukaryotic genomes. Mob DNA. 2015; 6:11. [PubMed: 26045719]
43. Thisse C, Thisse B. High-resolution in situ hybridization to whole-mount zebrafish embryos. Nat Protoc. 2008; 3:59–69. [PubMed: 18193022]
44. Carreira-Rosario A, Bhargava V, Hillebrand J, Kollipara RK, Ramaswami M, Buszczak M. Repression of Pumilio Protein Expression by Rbfox1 Promotes Germ Cell Differentiation. Dev Cell. 2016; 36:562–571. [PubMed: 26954550]

45. Jeske M, Bordi M, Glatt S, Muller S, Rybin V, Muller CW, Ephrussi A. The Crystal Structure of the *Drosophila* Germline Inducer Oskar Identifies Two Domains with Distinct Vasa Helicase- and RNA-Binding Activities. Cell Rep. 2015; 12:587–598. [PubMed: 26190108]

46. Costes SV, Daelemans D, Cho EH, Dobbin Z, Pavlakis G, Lockett S. Automatic and quantitative measurement of protein-protein colocalization in live cells. Biophys J. 2004; 86:3993–4003. [PubMed: 15189895]

47. Ephrussi A, Dickinson LK, Lehmann R. Oskar organizes the germ plasm and directs localization of the posterior determinant nanos. Cell. 1991; 66:37–50. [PubMed: 2070417]

48. Sogame N, Kim M, Abrams JM. Drosophila p53 preserves genomic stability by regulating cell death. Proc Natl Acad Sci U S A. 2003; 100:4696–4701. [PubMed: 12672954]

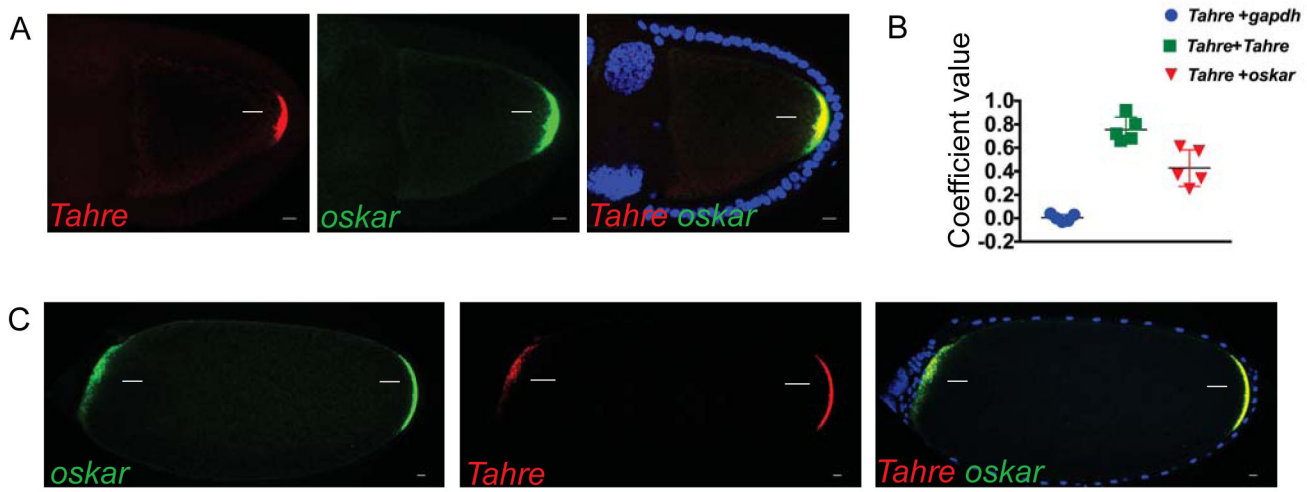

Figure 1. *Tahre* transposons mimic a germ plasm determinant

A, confocal images of the simultaneous *in situ* hybridization of *Tahre* fluorescently labeled with Quasar 570, *oskar* 670 and their merge in *Drosophila* egg chambers of $p53^{-/-}$ ovaries with maximum Z-series projections spanning 5 μm in oocytes at stages 9–10. Scale bars: 10 μm. (Blue) DAPI counterstain. Arrows indicate germ plasm associated signal. (B) Co-localization of *Tahre* RNAs with *oskar* RNAs was quantified using automated image analyses. Controls included probes for *gapdh* and differentially labeled *Tahre* probes (see STAR Methods). n=5 egg chambers. C, confocal images of *in situ* co-hybridizations using *oskar* and *Tahre* probes (as in A) on stage 14 egg chambers from animals expressing the transgene *oskar-bcd*3′UTR ovaries in the $p53^{-/-}$ background. Note that *Tahre* RNAs mirror *oskar* RNAs, localizing to both the native (rightward arrows) and ecoptic germ plasms (leftward arrows) in these bipolar oocytes. See also Figure S1 and STAR Methods.

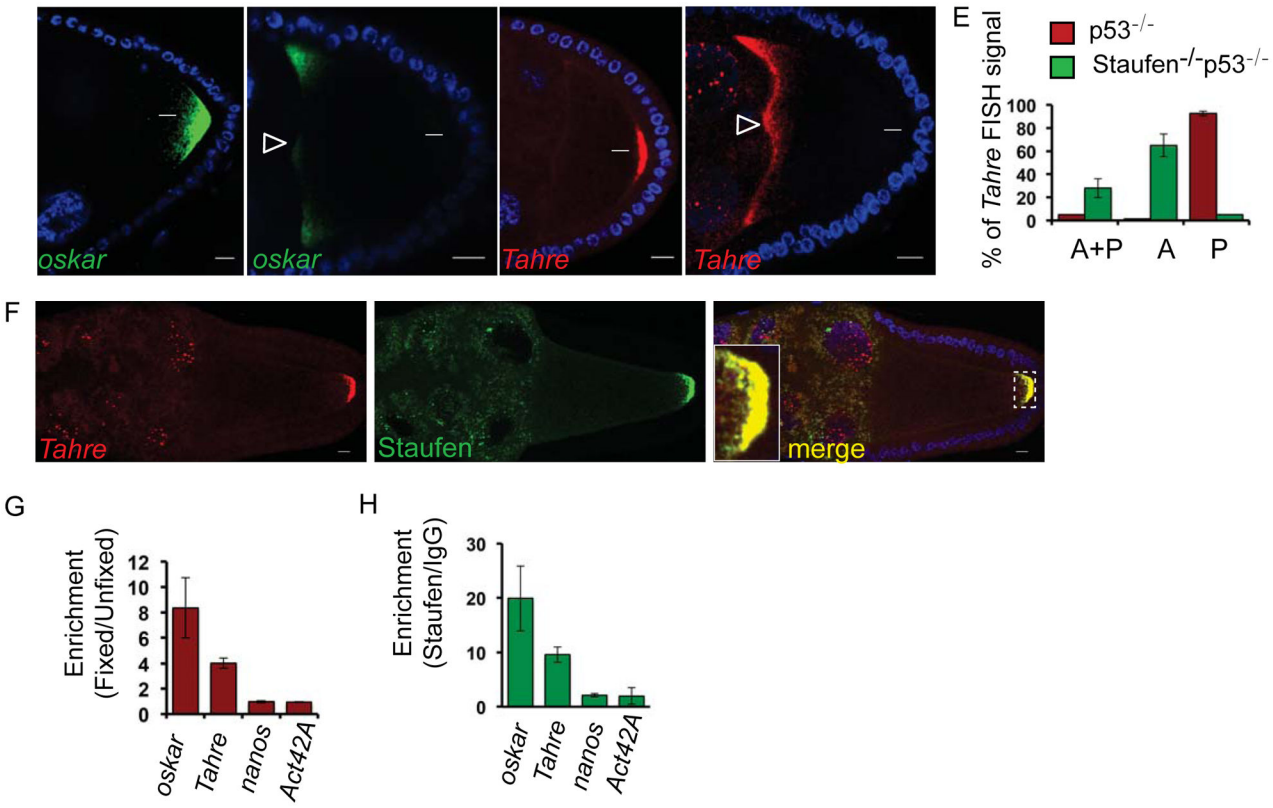

Figure 2. *Tahre* migration to the germ plasm requires *oskar* localization machinery

In situ hybridizations for *oskar* and *Tahre* on $p53^{-/-}$ (A and C respectively) and $Staufen^{-/-}$ $p53^{-/-}$ (B and D respectively) egg chambers that were DAPI counterstained (Blue). Arrows indicate germ plasm region. The percentage of egg chambers exhibiting *Tahre* FISH signal at the anterior and posterior (A+P), anterior only (A) and posterior only (P) poles of stages 9 egg chambers of $p53^{-/-}$ and $Staufen^{-/-}$ $p53^{-/-}$, were quantified from three biological replicates and are represented in bar graphs (E), n=50. Error bars represent ±SD. Note that in Staufen mutant oocytes, neither *oskar* nor *Tahre* localize at the posterior pole and, instead, these RNAs are stalled at the anterior pole (indicated by open arrow heads). Scale bar: 10 μm. Note that *Tahre* retroelements were similarly delocalized in egg chambers depleted for kinesin or Tm1C, see Supplemental Figures S3D and E. F show that *Tahre* transcripts co-associate with Staufen in the germ plasm (inset). *Tahre in situ* hybridization on GFP-Staufen; $p53^{-/-}$ ovaries depicting localization of *Tahre*, GFP-Staufen and merged. DAPI counterstain (Blue). Scale bar: 10 μm. (G, H) *Tahre* transcripts physically associate with Staufen. RIP assays were performed in formaldehyde fixed and unfixed $p53^{-/-}$ ovaries using IgG controls and Staufen antibodies. Fold enrichment for binding of the indicated RNAs were calculated relative to unfixed samples (G) or samples precipitated with IgG (H). Note that like the positive control *oskar, Tahre* transcripts were significantly enriched by precipitation of Staufen. For negative controls, *nanos* and *act42A* RNAs were used. Bar graphs are averages of three biological replicates. Error bars represent ±SD. See also Figures S2 and S3.

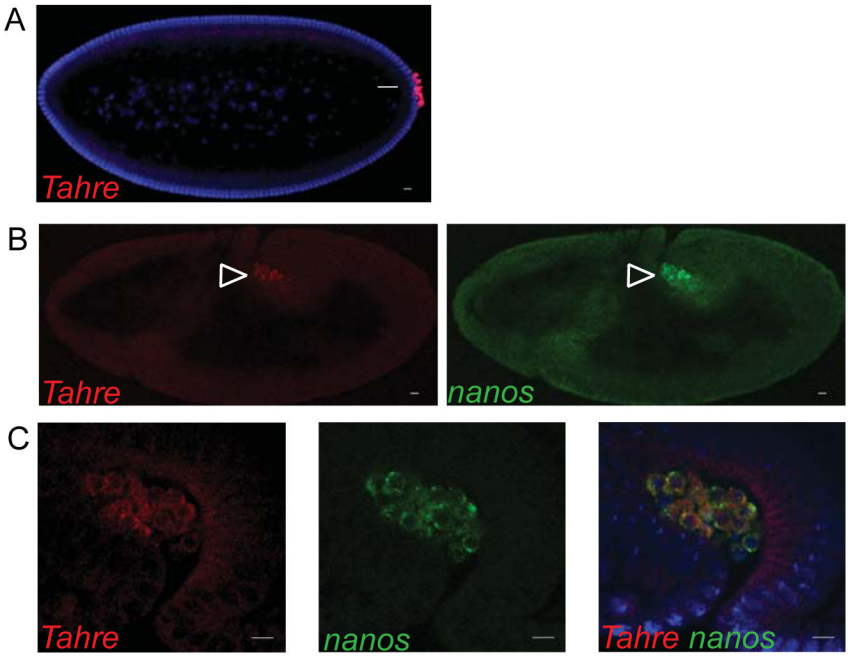

Figure 3. *Tahre* elements from the oocyte germ plasm persist in the embryonic germline

In (A), *Tahre* RNAs localize to the germline progenitors, the pole cells (arrow) of 0–3 hr $p53^{-/-}$ embryos. (B) *in situ* hybridizations reveal that *Tahre* localizes to the gonads (arrowheads) of later staged $p53^{-/-}$ embryos (stage 8), similar to the *nanos* marker. (C) Magnified images of *Tahre*, *nanos* and their merge. DAPI counterstain (Blue). Scale bars: 10 μm. See also Figure S4.

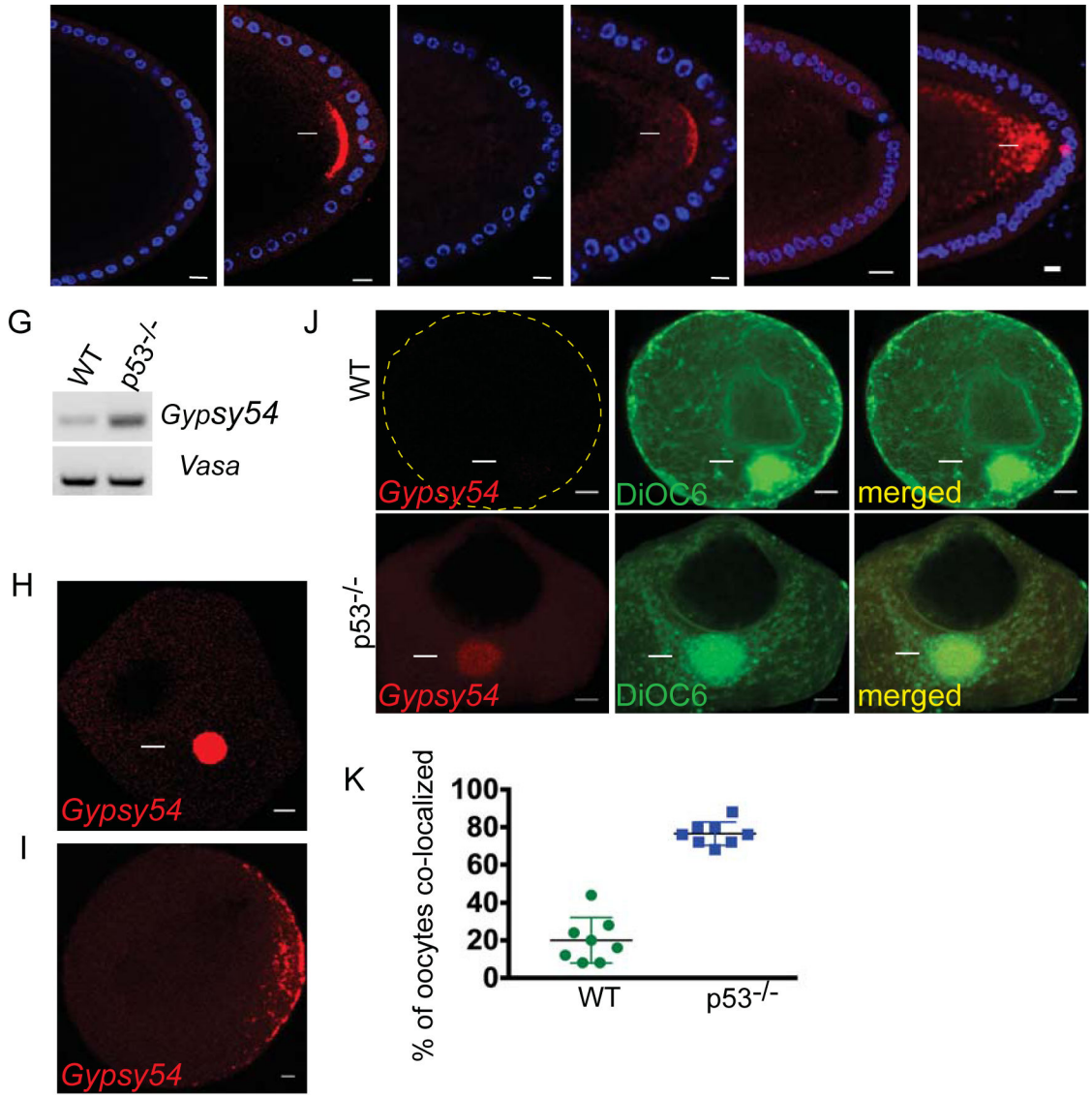

Figure 4. Germ plasm localization is conserved in invertebrates and vertebrates

Patterns of other retrotransposons in the fly oocyte were profiled by *in situ* hybridization. Examples of *Tahre* (A and B), *Burdock* (C and D), *HeT-A* (E and F) on WT and $p53^{-/-}$ oocytes are shown. DAPI counterstain (Blue). Like *Tahre*, *Burdock* and *HeT-A* RNAs also localized to the germ plasm region (arrows). Scale bars: 10 μm. G–K illustrate that *Gypsy54* localizes to the germ plasm of zebrafish oocytes. (G) RT-PCR analysis of *Gypsy54* and *vasa* (loading control) from WT and $p53^{-/-}$ zebrafish ovaries. (J–I) shows *in situ* hybridizations for *Gypsy54* RNA (red) on WT and $p53^{-/-}$ oocytes. Arrows point to the Balbiani body, the presumptive germ plasm of stage I oocytes (H). The arrowhead in (I) indicates the germ plasm at the cortical region of stage II oocytes. DiOC6 (green) was used to label the Balbiani body (J, arrow) in $p53^{-/-}$ and WT oocytes. Images are single optical sections. The scatter plot in (K) shows percentages of DiOC6-stained Balbiani bodies that were also positive for *Gypsy54* RNA. See also Figure S4 and See STAR Method.